



Structural, thermal and optical characterization of an organic NLO material—Benzaldehyde thiosemicarbazone monohydrate single crystals

R. Santhakumari^a, K. Ramamurthi^{b,*}

^a Department of Physics, Govt. Arts College for Women, Pudukkottai 622 001, Tamil Nadu, India

^b Crystal Growth and Thin Film Laboratory, School of Physics, Bharathidasan University, Tiruchirappalli 620 024, Tamil Nadu, India

ARTICLE INFO

Article history:

Received 3 June 2010

Received in revised form

13 November 2010

Accepted 30 November 2010

PACS:

81.10.Dn

61.66.Hq

65.60.+a

42.65.Ky

Keywords:

Characterization

Growth from solution

Organic compound

Nonlinear optical material

ABSTRACT

Single crystals of the organic NLO material, benzaldehyde thiosemicarbazone (BTSC) monohydrate, were grown by slow evaporation method. Solubility of BTSC monohydrate was determined in ethanol at different temperatures. The grown crystals were characterized by single crystal X-ray diffraction analysis to determine the cell parameters and by FT-IR technique to study the presence of the functional groups. Thermogravimetric and differential thermal analyses reveal the thermal stability of the crystal. UV–vis–NIR spectrum shows excellent transmission in the region of 200–1100 nm. Theoretical calculations were carried out to determine the linear optical constants such as extinction coefficient and refractive index. Further the optical nonlinearities of BTSC have been investigated by Z-scan technique with He–Ne laser radiation of wavelength 632.8 nm. Mechanical properties of the grown crystal were studied using Vickers microhardness tester. Second harmonic generation efficiency of the powdered BTSC monohydrate was tested using Nd:YAG laser and it is found to be ~5.3 times that of potassium dihydrogen orthophosphate.

© 2010 Elsevier B.V. All rights reserved.

1. Introduction

The overwhelming success of molecular engineering on controlling nonlinear optical (NLO) properties has attracted the attention of the researchers to search for a variety of new types of nonlinear optical materials [1] and to improve the NLO efficiency of the known materials. Organic molecules containing π electron conjugation systems asymmetricized by the electron donor and acceptor groups are highly polarizable entities for NLO applications [2]. The donor/acceptor of benzene derivatives can produce high molecular nonlinearity. Nonlinear optical materials, which can generate highly efficient second harmonic blue–violet, are of great interest for various applications including high speed optical communication, wireless optical computing, optical parallel information processing, optical disk data storage, laser fusion reactions, laser remote sensing, color display and medical diagnostics [3–5]. Recently there has been considerable interest in the co-ordination chemistry of aryl hydrazones such as semicarbazones, thiosemicarbazones and guanil hydrazones due to their importance for drug design [6], organocatalysis and for the preparation of hetero

cyclic rings [7]. Further extensive electron delocalization reported in these types of structures helps the thiosemicarbazone complexes to acquire second harmonic generation (SHG) efficiency [8–11]. Gu and Zhu [12] have reported on the three dimensional crystal and molecular structure of benzaldehyde thiosemicarbazone (BTSC) monohydrate. The crystal belongs to the well known non-centrosymmetric orthorhombic system with space group $P2_1 2_1 2_1$, thus satisfying the requirements for second order NLO activities. To our knowledge no systematic studies on the growth and characterization of the benzaldehyde thiosemicarbazone monohydrate have been made. Hence, in this investigation we report for the first time on the bulk growth and characterization of BTSC monohydrate single crystals.

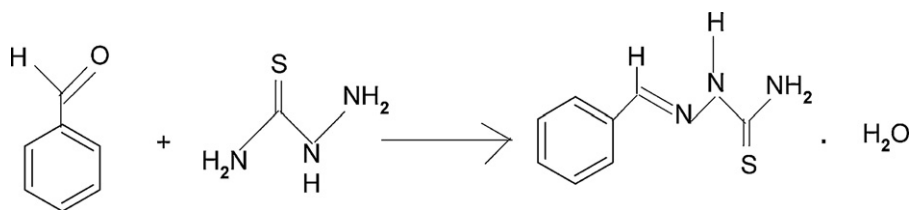
2. Experimental

2.1. Synthesis and solubility

The BTSC monohydrate was synthesized following the procedure given by Gu and Zhu [12] by reacting benzaldehyde and thiosemicarbazide in 100 ml flask in the presence of aqueous medium. After refluxing it for 2 h at 100 °C the mixture was allowed to cool slowly to room temperature which yielded colorless crystalline powder solid of the compound. The reaction is

* Corresponding author. Tel.: +91 431 2407057.

E-mail address: krmurthin@yahoo.co.in (K. Ramamurthi).



Scheme 1.

depicted in Scheme 1. Repeated recrystallization of BTSC monohydrate from ethanol was carried out to improve the purity of the compound. As a first step towards crystallization, the selection of suitable solvent is essential for the growth of good quality single crystals [13,14]. The solubility of BTSC monohydrate was determined at five different temperatures, viz., 25, 30, 35, 40 and 45 °C. The solubility at 25 °C was determined by dissolving the BTSC salt in 100 cm³ ethanol taken in an air-tight container with continuous stirring. After attaining the saturation the concentration of the solute was estimated gravimetrically. The same procedure was repeated to estimate the solubility at different temperatures [15] and the results are presented in Fig. 1.

2.2. Crystal growth

The purified colorless crystalline sample of BTSC monohydrate was dissolved thoroughly in ethanol at 30 °C to form the saturated solution. The pH of the solution was about 4. The solution of 50 ml was taken in a beaker and was properly sealed and placed in a constant temperature bath. The solvent was allowed to evaporate slowly at room temperature. Well defined crystals with good transparency were appeared in the beaker in a growth period of 10 days. One of the best crystals was selected as the seed crystal and inserted into a 100 ml beaker containing the solution of pH ~ 4 and placed in a constant temperature bath maintained at 30 °C. Single crystal of size 10 mm × 10 mm × 3 mm was harvested by slow evaporation method in a growth period of 25 days. The as-grown crystal is shown in Fig. 2.

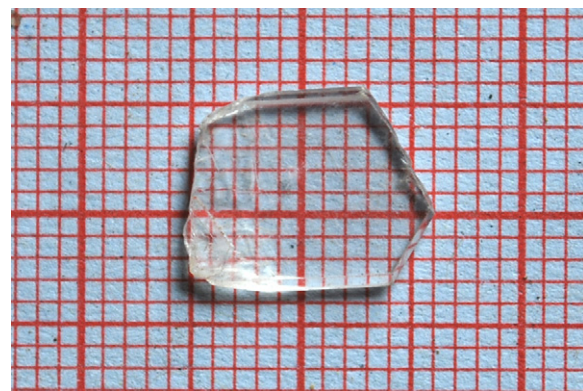


Fig. 2. The as-grown single crystal of BTSC monohydrate.

3. Results and discussion

3.1. Single crystal X-ray diffraction

The X-ray diffraction (XRD) data were collected using a computer-controlled Enraf Nonius-CAD 4 single crystal X-ray diffractometer. Single crystal of suitable size was selected for the X-ray diffraction analysis and the unit cell parameters were determined using 25 reflections. XRD results show that BTSC monohydrate crystal belongs to the orthorhombic system and the unit cell parameters obtained are in good agreement with the reported values of Gu and Zhu [12] (Table 1). It has been observed that BTSC crystal belongs to the most popular space group of $P2_12_12_1$, with molecules containing a chiral centre which allow maximal contribution from the microscopic molecular nonlinearity to the macroscopic crystal nonlinearity [16].

3.2. FT-IR spectral analysis

Fourier transform infrared (FTIR) spectrum of BTSC monohydrate was recorded using Perkin Paragon-500 by KBr pellet technique between 400 cm⁻¹ and 4000 cm⁻¹ and is shown in Fig. 3. As expected, the peak corresponding to imine group (C=N) was observed at 1595 cm⁻¹, which confirms the formation of the imine bond between aldehyde and hydrazide. The peaks lying below 1500 cm⁻¹ could be due to C=N and N–N stretching vibration. As it is very broad, nearly all NH₂ groups in the crystal are expected

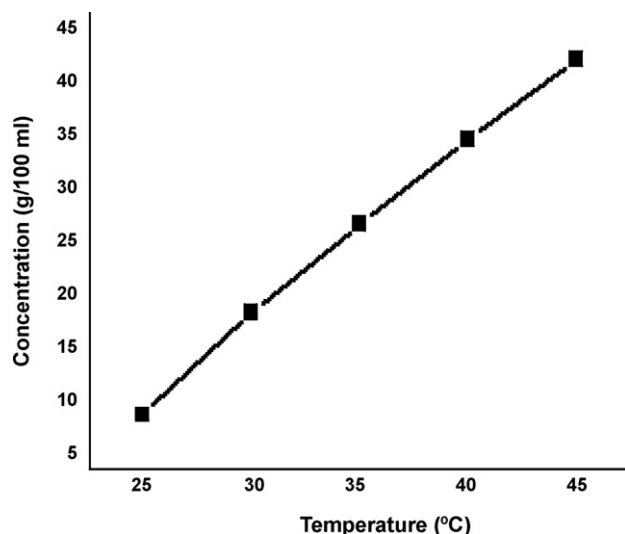


Fig. 1. Solubility curve of BTSC monohydrate.

Table 1

Unit cell parameters of BTSC monohydrate.

Cell parameters	Single crystal XRD (present work)	Single crystal XRD [12]
<i>a</i> (Å)	6.240(2)	6.1685(10)
<i>b</i> (Å)	7.5820(10)	7.6733(12)
<i>c</i> (Å)	21.129(36)	21.131(2)
Volume (Å ³)	998.3(9)	1000.2(2)
Orthorhombic system		

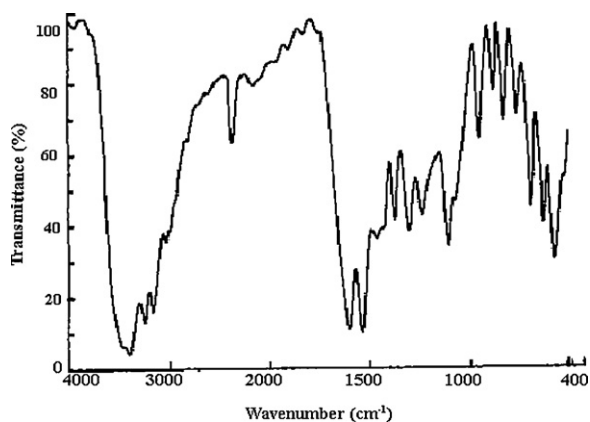


Fig. 3. FT-IR spectrum of BTSC monohydrate.

to be in hydrogen bonding interaction with neighbouring groups [17]. The C–H stretching absorption, a weak absorption, is observed at 3026 cm^{-1} [18]. The C=S stretch of thiosemicarbazide moiety is observed at 1100 cm^{-1} [19]. Absence of characteristic aldehyde band at 2720 cm^{-1} indicates that there is no aldehyde group in the final product.

3.3. Linear and nonlinear optical properties

The grown crystals were subjected to spectral analysis for studying the linear optical properties. The optical absorption spectrum of BTSC monohydrate crystal of 2 mm thickness was recorded in the range of 200–1100 nm using Varian Cary 5E UV–vis–NIR spectrophotometer (Fig. 4). The lower cut off of BTSC monohydrate is observed $\sim 370\text{ nm}$ and the crystal is found to be transparent in the region of $\sim 400\text{--}1100\text{ nm}$, an essential parameter required for frequency doubling process [20]. The hump at 220 nm is due to the electronic excitation of the aromatic compound containing sulfur and nitrogen [21].

The optical absorption coefficient (α) was calculated using the following relation

$$\alpha = \frac{2.303 \log(1/T)}{d} \quad (1)$$

where T is the transmittance and d is the thickness of the crystal. The various other optical constants were calculated using the following theoretical formulae [22,23].

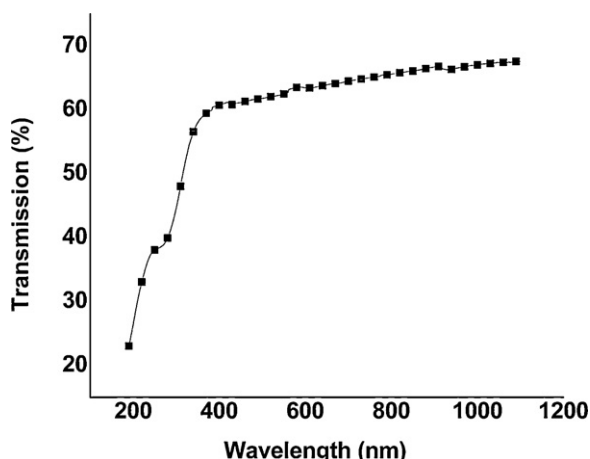


Fig. 4. UV–vis–NIR spectrum of BTSC monohydrate.

The extinction coefficient (K) is obtained in terms of the absorption coefficient,

$$K = \frac{\lambda\alpha}{4\pi} \quad (2)$$

where λ is the wavelength.

The reflectance (R) in terms of absorption coefficient is derived from the relation,

$$R = \frac{\sqrt{1 \pm (1 - \exp(-\alpha d) + \exp(\alpha d))}}{1 + \exp(-\alpha d)} \quad (3)$$

and the linear refractive index (n) is given by

$$n = \frac{-(R+1) \pm \sqrt{(-3R+10R-3)}}{2(R-1)}. \quad (4)$$

Also the complex dielectric constant is given by the relation,

$$\varepsilon_c = \varepsilon_r + \varepsilon_i \quad (5)$$

ε_r and ε_i are the real and imaginary part of the dielectric constant respectively. The real and imaginary dielectric constants are related to the refractive index and extinction coefficient as given below,

$$\varepsilon_r = n^2 - K^2 \quad (6)$$

$$\varepsilon_i = 2nK \quad (7)$$

The optical conductivity (σ_{op}) is a measure of the frequency response of the material when irradiated with light

$$\sigma_{op} = \frac{\alpha nc}{4\pi} \quad (8)$$

where c is the velocity of light. The electrical conductivity (σ_e) can also be estimated by optical method using the relation

$$\sigma_e = \frac{2\lambda\sigma_{op}}{\alpha} \quad (9)$$

The Z-scan is a simple and popular experimental technique to measure the intensity dependent third order nonlinear susceptibility of the materials. It allows the simultaneous measurement of both the nonlinear refractive index and the nonlinear absorption coefficient. In this method, the sample is translated in the Z-direction along the axis of a focused Gaussian beam from the He–Ne laser at 632.8 nm and the far field intensity is measured as a function of the sample position. The schematic diagram of Z-scan technique is as shown in Fig. 5. By properly monitoring the transmittance change through a small aperture at the far field position (closed aperture), one is able to determine the amplitude of the phase shift. By moving the sample through the focus and without placing an aperture at the detector (open aperture) one can measure the intensity dependent absorption of the sample. When both the methods (open and closed) are used for the measurements, the ratio of the signals determines the nonlinear refraction of the sample.

The recorded transmission spectrum of BTSC shows the lower cutoff wavelength at 370 nm and a wide transparency in the entire visible region which makes the material suitable for second harmonic generation. The energy dependence of the absorption coefficient suggests the occurrence of direct band gap and hence it obeys the relation for high photon energy,

$$(\alpha h\nu)^2 = A(h\nu - E_g) \quad (10)$$

where E_g is the optical band gap and A is a constant. The variation of $(\alpha h\nu)^2$ vs $h\nu$ in the fundamental absorption region is plotted in Fig. 6 and E_g is evaluated by the extrapolation of the linear part. The band gap is found to be 3.6 eV.

From the recorded absorption spectra, the linear optical constants of BTSC were calculated and the variation of optical constants as a function of photon energy is plotted (Figs. 7–10). The refractive

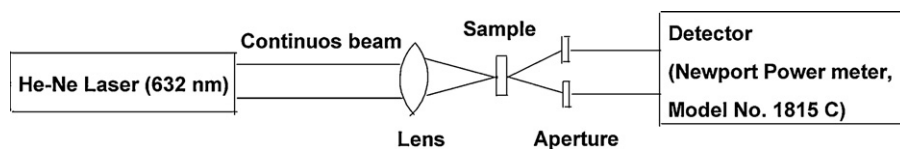


Fig. 5. Experimental set up for Z-scan.

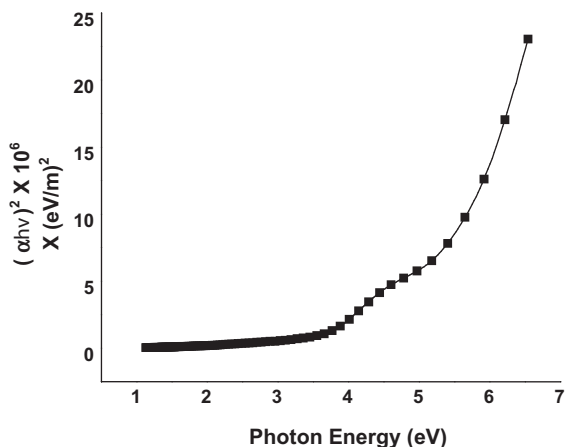
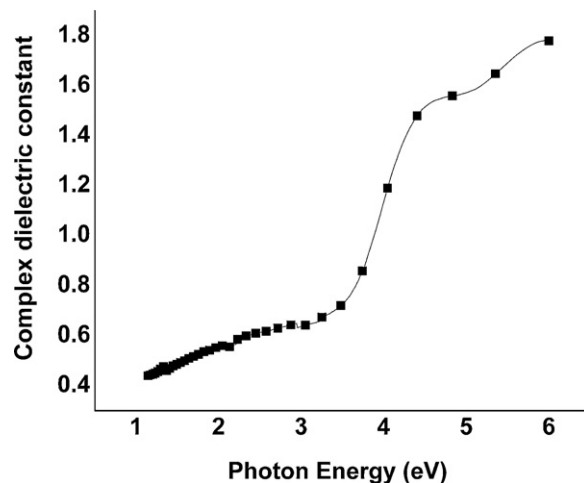
Fig. 6. $(\alpha h\nu)^2$ vs $h\nu$.

Fig. 9. Dielectric constant as a function of photon energy.

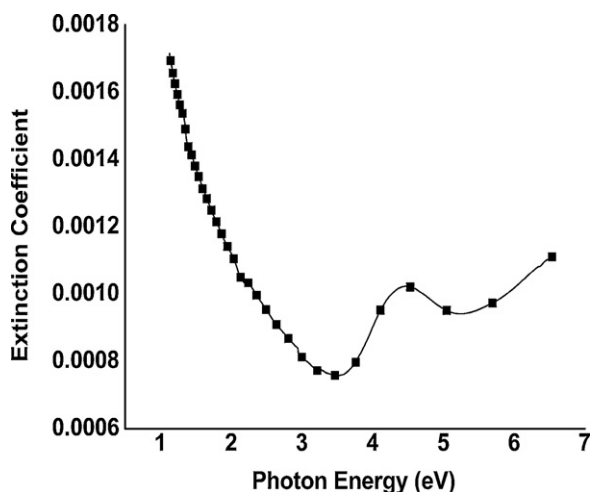


Fig. 7. Extinction coefficient as a function of photon energy.

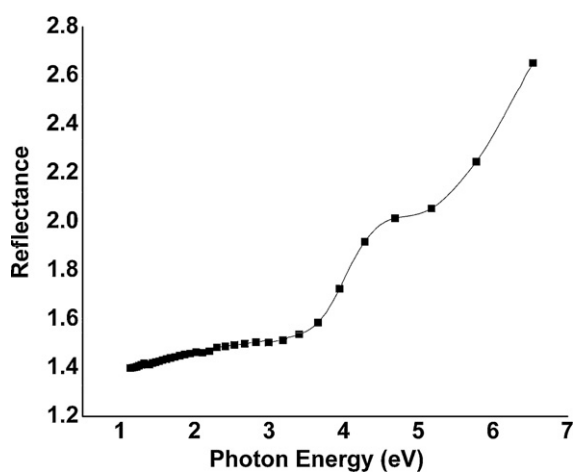


Fig. 8. Reflectance as a function of photon energy.

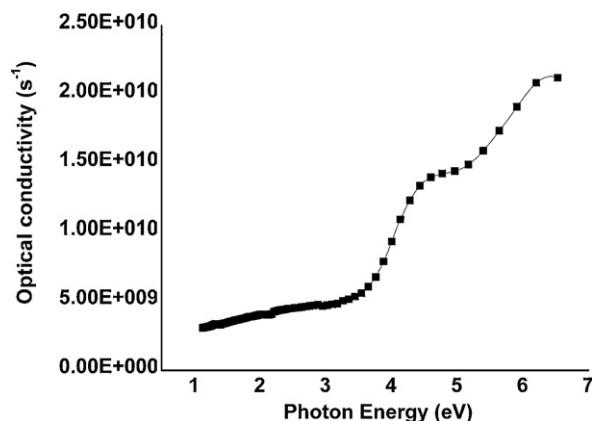


Fig. 10. Optical conductivity as a function of photon energy.

index of the material at 211 nm is 1.332. Also the extinction coefficient shows exponential decay as the photon energy increases. Refractive index being the measure of percentage of intensity of light reflected, the reflectance shows an increasing value along the photon energy. From Figs. 7 and 8, it is clear that the extinction coefficient and the reflectance depend upon the absorption coefficient. The internal energy of the device depends on this absorption coefficient. The high transmission, low absorbance, low reflectance and low refractive index of BTSC in the UV–vis region makes the material a prominent one for antireflection coating in solar thermal devices and nonlinear optical applications. The low extinction value (10^{-3}) and electrical conductivity ($10^2 (\Omega \text{ cm})^{-1}$) of the present work show the semiconducting nature of the material. The high magnitude of optical conductivity (10^{10} s^{-1}) confirms the presence of very high photo response nature of the material [22]. This makes the material more prominent for device applications in information processing and computing. From Figs. 9 and 10, the lower dielectric constant and the higher optical response suggest the better conversion efficiency of the material. Thus linear optical properties of

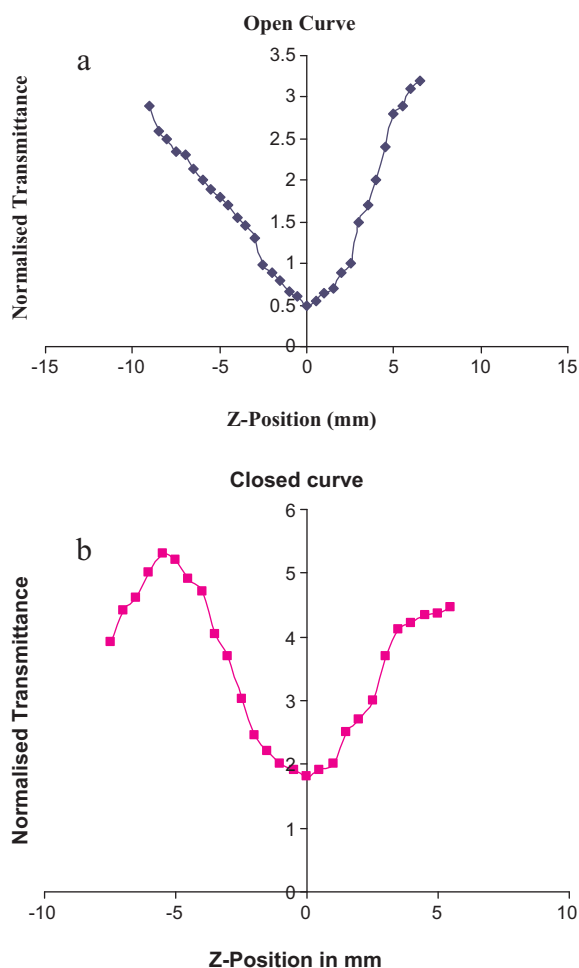


Fig. 11. (a) Z-scan open curve. (b) Z-scan closed curve.

BTSC confirm the material suitability for NLO and semiconducting applications.

The third order nonlinear refractive index and the nonlinear absorption coefficient were evaluated by the Z-scan measurements (Fig. 11a and b). A spatial distribution of the temperature in the crystal surface is produced due to the localized absorption of a tightly focused beam propagating through the absorbing sample. Hence a spatial variation of the refractive index is produced which acts as a thermal lens resulting in the phase distortion of the propagating beam. The difference between the peak and valley transmission (ΔT_{p-v}) is written in terms of the on axis phase ($|\varphi_0|$) shift at the focus as,

$$\Delta T_{p-v} = 0.406(1 - S)^{0.25} |\varphi_0| \quad (11)$$

where S is the aperture linear transmittance and is calculated using the relation

$$S = 1 - \exp\left[\frac{-2r_a^2}{\omega_a^2}\right] \quad (12)$$

where r_a is the radius of aperture and ω_a is the beam radius at the aperture. The nonlinear refractive index is given by

$$n_2 = \frac{\Delta\varphi}{KI_0L_{\text{eff}}} \quad (13)$$

where $K = 2\pi/\lambda$ (λ is the laser wavelength), I_0 is the intensity of the laser beam at the focus ($Z=0$), $L_{\text{eff}} = [1 - \exp(-\alpha L)]/\alpha$, is the effective thickness of the sample, α is the linear absorption and L is the thickness of the sample. From the open aperture Z-scan data, the

Table 2

Measurement details and the results of the Z-scan technique.

Laser beam wavelength	632.8
Focal length of the lens	24 cm
Optical path length	175 cm
Beam radius of the aperture (ω_a)	4 mm
Aperture radius (r_a)	4 mm
Sample thickness (l)	1.7 mm
Beam radius (ω_l)	3 mm
Effective thickness (L_{eff})	1.69 mm
Linear absorption coefficient	0.625
Nonlinear refractive index (n_2)	$-3.126 \times 10^{-8} \text{ cm}^2/\text{W}$
Nonlinear absorption coefficient (β)	$4.076 \times 10^{-3} \text{ cm/W}$
Real part of the third-order susceptibility [$Re(\chi^{(3)})$]	$3.27 \times 10^{-6} \text{ esu}$
Imaginary part of the third-order susceptibility [$Im(\chi^{(3)})$]	$2.15 \times 10^{-6} \text{ esu}$
Third-order susceptibility ($\chi^{(3)}$)	$3.915 \times 10^{-6} \text{ esu}$

nonlinear absorption coefficient is estimated from the equation

$$\beta = \frac{2\sqrt{2}\Delta T}{I_0L_{\text{eff}}} \quad (14)$$

where ΔT is the one valley value at the open aperture Z-scan curve. The value of β will be negative for saturable absorption and positive for two photon absorption. The real and imaginary parts of the third order nonlinear optical susceptibility $\chi^{(3)}$ are defined by

$$Re(\chi^{(3)}) \text{ (esu)} = \frac{10^{-4}}{\pi} (\varepsilon_0 c^2 n_0^2 n_2) \text{ (cm}^2/\text{W)} \quad (15)$$

$$Im(\chi^{(3)}) \text{ (esu)} = \frac{10^{-2}}{4\pi^2} (\varepsilon_0 c^2 n_0^2 n_2) \text{ (cm/W)} \quad (16)$$

where ε_0 is the vacuum permittivity, n_0 is the linear refractive index of the sample and c is the velocity of light in vacuum. Table 2 portrays the experimental details and the results of the Z-scan technique for BTSC. The calculated value of the nonlinear refractive index n_2 is $-3.126 \times 10^{-8} \text{ cm}^2/\text{W}$. From the open aperture Z-scan curve, it can be concluded that as the minimum lies near the focus ($Z=0$), the nonlinear absorption is regarded as two photon absorption. The nonlinear absorption coefficient is found to be $4.076 \times 10^{-3} \text{ cm/W}$. The third order susceptibility of BTSC is $3.915 \times 10^{-6} \text{ esu}$.

3.4. Microhardness

Measurement of hardness is a useful nondestructive testing method to determine the hardness of the materials. The microhardness value correlates with other mechanical properties such as elastic constants and yield strength. The hardness of a material depends on different parameters such as lattice energy, Debye temperature, heat of formation and interatomic spacing [24,25]. According to Gong [26], during an indentation process, the external work applied by the indenter is converted into a strain energy component which is proportional to the volume of the resultant impression and a surface energy component found to be proportional to the area of the resultant impression. Vickers microhardness test was carried out on BTSC monohydrate single crystal using Vickers hardness tester fitted with pyramidal indenter. Several trials of indentation were carried out on the prominent (0 1 1) face of the crystal and the average diagonal length was calculated for an indentation time of 15 s. The Vickers hardness number is calculated using the relation

$$H_v = 1.8544 \frac{P}{d^2} \text{ kg/mm}^2 \quad (17)$$

where P is the applied load in kg and d is the average diagonal length of impression in mm. The variation of H_v with applied load for BTSC monohydrate crystal is shown in Fig. 12. Cracks were observed for loads more than 100 g. Work hardening coefficient n , a measure of

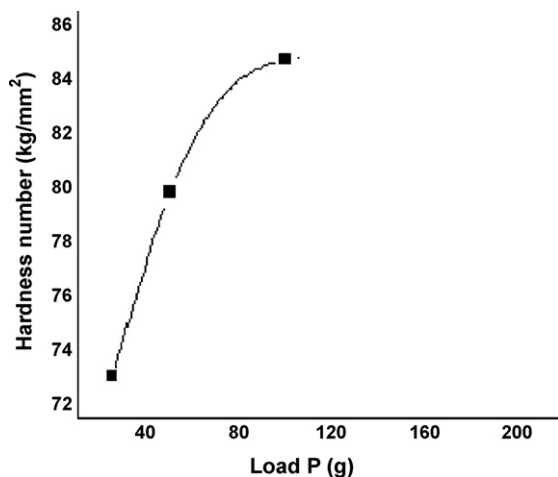


Fig. 12. The variation of hardness number vs load P .

the strength of the crystal, is computed from the plot of $\log P$ vs $\log d$. The plot of $\log P$ vs $\log d$ of BTSC monohydrate crystal yields a straight line and its slope, the work hardening index n , is found to be 2.08.

According to Meyer's law [27],

$$P = K_1 d^n \quad (18)$$

where K_1 is the standard hardness found out from the P vs d^n graph. It is known that the material takes some time to revert to elastic mode after the applied load is removed, so a correction x is applied to the observed d value [28]. Kick's law [29] may be modified as,

$$P = K_2(d+x)^2 \quad (19)$$

Simplifying Eqs. (18) and (19) become

$$d^{n/2} = \left(\frac{K_2}{K_1}\right)^{1/2} d + \left(\frac{K_2}{K_1}\right)^{1/2} x \quad (20)$$

The slope of $d^{n/2}$ versus d yields $(K_2/K_1)^{1/2}$ and the intercept is a measure of x . The fracture toughness (K_C) is given by

$$K_C = \frac{P}{\beta \times C^{3/2}} \quad (21)$$

where C is the crack length measured from the centre of the indentation mark to the crack tip, P is the applied load and geometrical constant $\beta = 7$ for Vicker's indenter. The brittleness index (B) is given by

$$B = \frac{H_V}{K_C} \quad (22)$$

The yield strength (σ_v) of the material can be found out using the relation

$$\sigma_v = \frac{H_V}{2.9} \left\{ [1 - (n-2)] \times \left[\frac{12.5(n-2)}{1 - (n-2)} \right]^{n-2} \right\} \quad (23)$$

From the Vicker's microhardness studies, it is observed that the hardness value increases up to a load of 100 g. Cracks developed around the indentation mark for loads above 100 g. The formation of cracks confirms the decrease in microhardness [30]. Onitsch [31] inferred that for hard materials the value of n lies between 1 and 1.6 and for soft materials it is above 1.6. Thus the BTSC monohydrate crystal comes under the soft materials category. The load dependent hardness parameters n , K_1 , K_2 , fracture toughness (K_C), brittleness index (B) and yield strength (σ_v) were calculated for the BTSC monohydrate crystal and are given in Table 3.

Table 3
Microhardness value obtained on the BTSC crystal.

Parameters	Values
n	2.08
K_1 (kg/mm)	27.7
K_2 (kg/mm)	30.16
K_C (g/ $\mu\text{m}^{3/2}$)	0.0535
B_i ($\text{m}^{-1/2}$)	1.58×10^8

3.5. Thermal analysis

Thermogram provides information about the thermal properties of materials [32]. The thermal stability of BTSC monohydrate crystal was studied by thermogravimetric analysis (TGA) and differential thermal analysis (DTA) using SDT Q600 V8.3 Build 101 instrument between the temperatures 50 °C and 1100 °C at a heating rate of 10 °C/min in nitrogen atmosphere (Fig. 13). The BTSC monohydrate sample weighing 1.745 mg was taken for the measurement. There are three weight losses noted in the thermogram. The earlier one is due to expulsion of water present in the crystal. The second and third major weight loss is observed just above 220 °C and 400 °C. It is due to decomposition of BTSC monohydrate crystal. The formation of minute quantities of decomposition residues is also noted in the thermogram. From the DTA curve it is observed that, the material is stable up to 153 °C, the melting point of the substance. The melting point, also measured directly using a GUNA melting point apparatus, confirmed this value. Above this point, the material begins to attain an endothermic transition and begins to decompose. The sharpness of this endothermic peak shows the good degree of crystallinity of the sample [33].

3.6. Nonlinear optical studies

Kurtz and Perry [34] second harmonic generation (SHG) test was performed to estimate the NLO efficiency of powdered BTSC monohydrate crystal. The grown single crystal of BTSC was powdered with a uniform particle size and then packed in a micro capillary of uniform bore and was illuminated using Spectra Physics Quanta Ray DHS2. Nd:YAG laser using the first harmonics output of 1064 nm with pulse width of 8 ns and repetition rate 10 Hz. The second harmonics signal, generated in the crystal was confirmed from the emission of green radiation by the crystal. A sample of potassium dihydrogen orthophosphate, also powdered to the same particle size as the experimental sample, used as a reference material in the present measurement. The SHG radiation of 532 nm green light was collected by a photomultiplier tube (PMT-Philips Photonics-

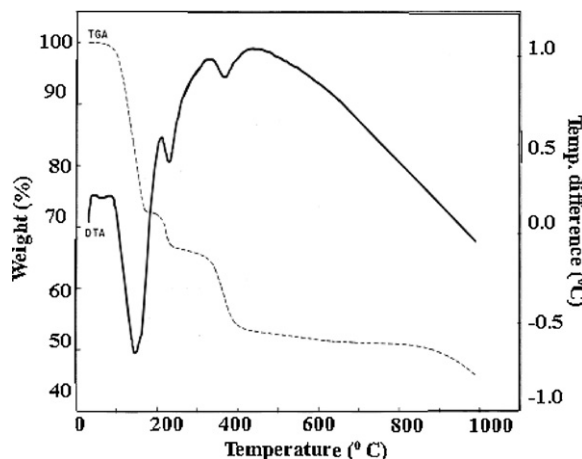


Fig. 13. TGA/DTA curves of BTSC monohydrate.

model 8563) after being monochromated (monochromator-model Triax-550) to collect only the 532 nm radiation. The optical signal incident on the PMT was converted into voltage output at the CRO (Tektronix-TDS 3052B). The input laser energy incident on the powdered sample was chosen to be 3.4 mJ. Powder SHG efficiency obtained for BTSC monohydrate is about 5.3 times that of potassium dihydrogen orthophosphate crystal. This may be due to the existence of intermolecular N–H...N and N–H...S hydrogen bonds and N–H...O and O–H...S hydrogen bonds due to water molecules in BTSC, which link the molecules into ribbons extended along the *a*-axis [12].

4. Conclusion

Well developed transparent benzaldehyde thiosemicarbazone monohydrate single crystal of dimensions 10 mm × 10 mm × 3 mm was grown by the slow evaporation technique at 30 °C. Determination of unit cell constants by the single crystal X-ray diffraction technique confirmed the identity of the synthesized material. FTIR spectral studies confirmed the presence of functional groups of BTSC monohydrate crystal. Optical transmittance window and the lower cut off wavelength identified through UV–vis–NIR spectrum reveal that BTSC monohydrate is a potential candidate for second harmonic generation. The high transmission, low absorbance, low reflectance and low refractive index of BTSC in the UV–vis–NIR make the material a prominent one for antireflection coating in solar thermal devices. Thus BTSC with many attracting linear and nonlinear optical properties is a suitable candidate for optoelectronic applications. Vickers microhardness study reveals the mechanical strength of the BTSC monohydrate crystal. TGA and DTA reveal that this compound is stable up to its melting point 153 °C. Second harmonic generation efficiency of the powdered BTSC monohydrate crystal is ~5.3 times that of potassium dihydrogen orthophosphate crystal.

Acknowledgments

The authors (RS and KR) thank to Dr. K. Panchanatheeswaran, Professor in Chemistry (Rtd), Bharathidasan University, Tiruchirappalli for fruitful discussion. Further one of the authors [RS] thank University Grants Commission, Government of India for financial assistance [File No. MRP 2976/2009 (RS)]. Authors thank Prof. D. Sastikumar, Department of Physics, NIT, Tiruchirappalli, for the support in recording the Z-scan measurements. The authors acknowledge Prof. P.K. Das, Department of Inorganic and Physical

Chemistry, Indian Institute of Science, Bangalore for extending the laser facilities for the SHG measurement.

References

- [1] G. Aka, F. Mougel, F. Auge, A. Kahn-Harari, D. Vivien, J.M. Benitez, J. Alloys Comp. 401 (2004) 303–304.
- [2] P. Tansuri, K. Tansuree, B. Gabriele, R. Lara, J. Cryst. Growth Des. 4 (2004) 743–747.
- [3] B.J. McArdle, J.N. Sherwood, A.C. Damask, J. Cryst. Growth 22 (1974) 193–200.
- [4] M. Aravindhan, K. Sankaranarayanan, K. Ramamurthy, C. Sanjeeviraja, P. Ramasamy, Thin Solid Films 477 (2005) 2–6.
- [5] S. Ayers, M.M. Faktor, D. Marr, J.L. Stevensons, J. Mater. Sci. 7 (1972) 31–33.
- [6] H. Beraldo, D. Gambino, Mini Rev. Med. Chem. 4 (2004) 31–39.
- [7] S. Bondock, K. Halifa, A.A. Fadda, J. Med. Chem. 42 (2007) 948–954.
- [8] D. Govanni, F.G. Giovanna, N. Mario, S. Paolo, Acta Crystallogr. B26 (1970) 1005–1009.
- [9] D. Govanni, F.G. Giovanna, N. Mario, S. Paolo, Acta Crystallogr. B25 (1969) 343–349.
- [10] D. Muharrem, O. Namik, Acta Crystallogr. E61 (2005) o880–o883.
- [11] D. Muharrem, O. Namik, Acta Crystallogr. C62 (2005) o13–o15.
- [12] S.-J. Gu, K.-M. Zhu, Acta Crystallogr. E64 (2008) o1597–o1604.
- [13] J.N. Sherwood, Pure Appl. Opt. 7 (1998) 229–238.
- [14] A. Holden, P. Singer, Crystals and Crystal Growing, Double Day and Company Inc., New York, 1960.
- [15] T. Balakrishnan, K. Ramamurthi, Spectrochim. Acta 68A (2007) 362–363.
- [16] E. Pidcock, A Chiral Molecules is Non-centrosymmetric Space Groups, 2005, doi:10.1039/b505236.
- [17] R. Ramesh Babu, N. Vijayan, R. Gopalakrishnan, P. Ramasamy, J. Cryst. Growth 240 (2002) 545–548.
- [18] R.M. Silverstein, F.X. Webster (Eds.), Spectrometric Identification of Organic Compounds, sixth ed., John Wiley and Sons, Inc., Canada, 1998, pp. 91–103.
- [19] Y.R. Sharma, Elementary Organic spectroscopy, S. Chand, New Delhi, 2009, p. 105.
- [20] C.N.R. Rao, Ultraviolet and Visible Spectroscopy of Organic Compound, Prentice Hall Pvt. Ltd., New Delhi, 1984, pp. 60–66.
- [21] G.R. Chatwal, S.K. Anand, Atomic and Molecular Spectroscopy, fifth ed., Himalaya Publishing House, 2004, p. 2.154.
- [22] P.A. Heinkhen, Afr. Phys. Rev. 2 (2008) 68.
- [23] J.I. Pankove, Optical Processes in Semiconductors, Prentice hall, New York, 1971, p. 412.
- [24] C. Vesta, R. Uthrakumar, C. Justin Raj, A. Jonie Varjula, J. Mary Linet, S. Jerome Das, J. Mater. Sci. Technol. 23 (2007) 855–859.
- [25] R. Uthrakumar, C. Vesta, C. Justin Raj, S. Krishnan, S. Jerome Das, Curr. Appl. Phys. 10 (2010) 548–552.
- [26] J. Gong, J. Mater. Sci. Lett. 19 (2005) 515–517.
- [27] Meyer, Some Aspects of the Hardness of Metals, PhD thesis, Draft, 1951.
- [28] H. Li, R.C. Bradt, J. Hard Mater. 3 (1993) 403–419.
- [29] F. Kick, D. Gasetzder, proportionalen widerstande Und Science anwendung, Felix, Leipzig, 1885.
- [30] C. Hays, E.G. Kendall, Metallography 6 (1973) 275–282.
- [31] E.M. Onitsch, Mikroskope 95 (1950) 12–14.
- [32] C.M. Earnet, Anal. Chem. 56 (1984) 1471A–1486A.
- [33] Y.Le. Fur, R. Masse, M.Z. Cherkaoui, J.F. Nicoud, Z. Kristallogr. 210 (1995) 856–860.
- [34] S.K. Kurtz, T.T. Perry, J. Appl. Phys. 39 (1968) 3798–3813.